Sports, Science and Technology of Japan (MEXT, No. 21390532 and 21659462), and Research and Development Programs for Three-dimensional Complex Organ Structures from the New Energy and Industrial Technology Development Organization and for Resolving Critical Issues from Special Coordination Funds for Promoting Science and Technology (SCF) commissioned by MEXT.

REFERENCES

1. Asawa Y, Ogasawara T, Takahashi T, Yamaoka H, Nishizawa S, Matsudaira K, Mori Y, Takato T and Hoshi K (2009) Aptitude of auricular and nasoseptal chondrocytes cultured under a monolayer or three-dimensional condition for cartilage tissue engineering. *Tissue Eng Part A* **15**, 1109–1118.
2. Bakker VM and Johnston LE Jr (1985) The effect of Class II elastic forces on craniofacial growth in rats. *J Dent Res* **64**, 44–47.
3. Benya PD (1981) Two-dimensional CNBr peptide patterns of collagen types I, II and III. *Coll Relat Res* **1**, 17–26.
4. Brittberg M, Lindahl A, Nilsson A, Ohlsson C, Isaksson O and Peterson L (1994) Treatment of deep cartilage defects in the knee with autologous chondrocyte transplantation. *N Engl J Med* **331**, 889–895.
5. Freitas PH, Kojima T, Ubaidus S, Suzuki A, Li M, Yoshizawa M, Oda K, Maeda T, Kudo A, Saito C and Amizuka N (2007) Histochemical examinations on cortical bone regeneration induced by thermoplastic bioresorbable plates applied to bone defects of rat calvariae. *Biomed Res* **28**, 191–203.
6. Fujihara Y, Takato T and Hoshi K (2010) Immunological response to tissue-engineered cartilage derived from auricular chondrocytes and a PLLA scaffold in transgenic mice. *Biomaterials* **31**, 1227–1234.
7. Grigoriadis AE, Aubin JE and Heersche JN (1989) Effects of dexamethasone and vitamin D3 on cartilage differentiation in a clonal chondrogenic cell population. *Endocrinology* **125**, 2103–2110.
8. Jiao Y, Wang D, Han W and Hu J (1999) Phenotypic changes of mandibular condylar cartilage cells during subculture. *Hua Xi Kou Qiang Yi Xue Za Zhi* **17**, 355–357.
9. Kato Y and Gospodarowicz D (1984) Growth requirements of low-density rabbit costal chondrocyte cultures maintained in serum-free medium. *J Cell Physiol* **120**, 354–363.
10. Liu G, Kawaguchi H, Ogasawara T, Asawa Y, Kishimoto J, Takahashi T, Chung UI, Yamaoka H, Asato H, Nakamura K, Takato T and Hoshi K (2007) Optimal combination of soluble factors for tissue engineering of permanent cartilage from cultured human chondrocytes. *J Biol Chem* **282**, 20407–20415.
11. Malinin TI and Hornicek FJ (1997) Response of human chondrocytes cultured in vitro to human somatotropin, triiodothyronine, and thyroxine. *Transplant Proc* **29**, 2037–2039.
12. Maor G, Segev Y and Phillip M (1999) Testosterone stimulates insulin-like growth factor-I and insulin-like growth factor-I-receptor gene expression in the mandibular condyle—a model of endochondral ossification. *Endocrinology* **140**, 1901–1910.
13. Mohan N, Nair PD and Tabata Y (2009) A 3D biodegradable protein based matrix for cartilage tissue engineering and stem cell differentiation to cartilage. *J Mater Sci Mater Med* **20** Suppl 1, S49–S60.
14. Monsonego E, Halevy O, Gertler A, Hurwitz S and Pines M (1995) Growth hormone inhibits differentiation of avian epiphyseal growth-plate chondrocytes. *Mol Cell Endocrinol* **114**, 35–42.
15. Peterson L, Minas T, Brittberg M, Nilsson A, Sjögren-Jansson E and Lindahl A (2000) Two- to 9-year outcome after autologous chondrocyte transplantation of the knee. *Clin Orthop Relat Res* **374**, 212–234.
16. Rodd C, Jourdain N and Alini M (2004) Action of estradiol on epiphyseal growth plate chondrocytes. *Calcif Tissue Int* **75**, 214–224.
17. Schnabel M, Marlovits S, Eckhoff G, Fichtel I, Gotzen L, Vécsei V and Schlegel J (2002) De-differentiation-associated changes in morphology and gene expression in primary human articular chondrocytes in cell culture. *Osteoarthritis Cartilage* **10**, 62–70.
18. Shukunami C, Ohta Y, Sakuda M and Hiraki Y (1998) Sequential progression of the differentiation program by bone morphogenetic protein-2 in chondrogenic cell line ATDC5. *Exp Cell Res* **241**, 1–11.
19. Soule HD and McGrath CM (1986) A simplified method for passage and long-term growth of human mammary epithelial cells. *In Vitro Cell Dev Biol* **22**, 6–12.
20. Tadokoro M, Matsushima A, Kotobuki N, Hirose M, Kimura Y, Tabata Y, Hattori K and Ohgushi H (2012) Bone morphogenetic protein-2 in biodegradable gelatin and β-tricalcium phosphate sponges enhances the in vivo bone-forming capability of bone marrow mesenchymal stem cells. *J Tissue Eng Regen Med* **6**, 253–260.
21. Takahashi T, Ogasawara T, Kishimoto J, Liu G, Asato H, Nakatsuka T, Uchinuma E, Nakamura K, Kawaguchi H, Chung UI, Takato T and Hoshi K (2005) Synergistic effects of FGF-2 with insulin or IGF-1 on the proliferation of human auricular chondrocytes. *Cell Transplant* **14**, 683–693.
22. Takahashi T, Ogasawara T, Asawa Y, Mori Y, Uchinuma E, Takato T and Hoshi K (2007) Three-dimensional microenvironments retain chondrocyte phenotypes during proliferation culture. *Tissue Eng* **13**, 1583–1592.
23. Tanaka Y, Ogasawara T, Asawa Y, Yamaoka H, Nishizawa S, Mori Y, Takato T and Hoshi K (2008) Growth factor contents of autologous human sera prepared by different production methods and their biological effects on chondrocytes. *Cell Biol Int* **32**, 505–514.
24. Tanaka Y, Yamaoka H, Nishizawa S, Nagata S, Ogasawara T, Asawa Y, Fujihara Y, Takato T and Hoshi K (2010) The optimization of porous polymeric scaffolds for chondrocyte/atelocollagen based tissue-engineered cartilage. *Biomaterials* **31**, 4506–4516.
25. Uchiyama H, Yamato M, Sasaki R, Sekine H, Yang J, Ogiuchi H, Ando T and Okano T (2011) In vivo 3D analysis with micro-computed tomography of rat calvaria bone regeneration using periosteal cell sheets fabricated on temperature-responsive culture dishes. *J Tissue Eng Regen Med* **5**, 483–490.
26. Veilleux NH, Yannas IV and Spector M (2004) Effect of passage number and collagen type on the proliferative, biosynthetic, and contractile activity of adult canine articular chondrocytes in type I and II collagen-glycosaminoglycan matrices in vitro. *Tissue Eng* **10**, 119–127.
27. Watanabe H, Yamada Y and Kimata K (1999) Roles of aggrecan, a large chondroitin sulfate proteoglycan, in cartilage structure and function. *J Biochem* **124**, 687–693.
28. Wroblewski J and Edwall-Arvidsson C (1995) Inhibitory effects of basic fibroblast growth factor on chondrocyte differentiation. *J Bone Miner Res* **10**, 735–742.

29. Yamaoka H, Tanaka Y, Nishizawa S, Asawa Y, Takato T and Hoshi K (2010) The application of atelocollagen gel in combination with porous scaffolds for cartilage tissue engineering and its suitable conditions. *J Biomed Mater Res A* **93**, 123–132.
30. Yamaoka H, Asato H, Ogasawara T, Nishizawa S, Takahashi T, Nakatsuka T, Koshima I, Nakamura K, Kawaguchi H, Chung UI, Takato T and Hoshi K (2006) Cartilage tissue engineering using human auricular chondrocytes embedded in different hydrogel materials. *J Biomed Mater Res A* **78**, 1–11.
31. Yanaga H, Yanaga K, Imai K, Koga M, Soejima C and Ohmori K (2006) Clinical application of cultured autologous human auricular chondrocytes with autologous serum for craniofacial or nasal augmentation and repair. *Plast Reconstr Surg* **117**, 2019–2030.
32. Yanaga H, Imai K, Fujimoto T and Yanaga K (2009) Generating ears from cultured autologous auricular chondrocytes by using two-stage implantation in treatment of microtia. *Plast Reconstr Surg* **124**, 817–825.
33. Yokoi M, Hattori K, Narikawa K, Ohgushi H, Tadokoro M, Hoshi K, Takato T, Myoui A, Nanno K, Kato Y, Kanawa M, Sugawara K, Kobo T and Ushida T (2012) Feasibility and limitations of the round robin test for assessment of in vitro chondrogenesis evaluation protocol in a tissue-engineered medical product. *J Tissue Eng Regen Med* **6**, 550–558.
34. Yonenaga K, Nishizawa S, Akizawa M, Asawa Y, Fujihara Y, Takato T and Hoshi K (2010) The optimal conditions of chondrocyte isolation and its seeding in the preparation for cartilage tissue engineering. *Tissue Eng Part C* **16**, 1461–1469.
35. Yonenaga K, Nishizawa S, Akizawa M, Asawa Y, Fujihara Y, Takato T and Hoshi K (2010) Utility of NucleoCounter for the chondrocyte count in the collagenase digest of human native cartilage. *Cytotechnology* **62**, 539–545.
36. Yasuda T and Poole AR (2002) A fibronectin fragment induces type II collagen degradation by collagenase through an interleukin-1-mediated pathway. *Arthritis Rheum* **46**, 138–148.

頭頸部外科　22（2）：121～124，2012

顎顔面領域における骨軟骨再生医療の現状と展望

高戸　毅[1)]　星　和人[2)]　藤原夕子[2)]
西條英人[1)]　菅野勇樹[1)]　大久保和美[1)]
鄭　雄一[3)]　森　良之[1)]

要旨：顎顔面領域は四肢骨に比較して荷重負荷がかかりにくく，概して再建で必要とされる組織量も少ないことから，再生組織の移植に適した領域であると考えられる。しかし，人工骨や人工歯根など様々な生体材料を用いた治療法が確立しており，また大型の組織欠損に対しては，マイクロサージャリーによる組織再建やエピテーゼによる補綴も行われている。従って，顎顔面領域における再生医療の展開は，既存の医療を低侵襲治療として凌駕する，或いは，より卓越した治療効果を発揮することにより可能になると考える。本稿では，われわれのグループが開発し実用段階に達している骨・軟骨再生医療について，基礎と臨床の面から紹介する。
キーワード：骨軟骨再生医療，顎顔面領域，CT bone，インプラント型再生軟骨

Ⅰ．緒　言

再生医療とは，機能障害や機能不全に陥った生体組織・臓器に対して，細胞を積極的に利用して機能の再生をはかる医療であり，再生医療を利用した新たな治療法の開発に期待が高まっている。

再生医療の歴史は古く，1970年代にまで遡る。1993年には，ハーバード大学医学部子供病院の消化器外科医J P. Vacantiとマサチューセッツ工科大学の応用化学者R. Langerが生分解性高分子製の足場（スカフォールド）に細胞を播種し，成長因子の存在下で組織形成を誘導するというTissue Engineering（組織工学）の概念を提唱した。彼らが提唱する方法で作製されたマウスの背中に乗ったヒトの耳の写真は，世界のマスコミで広く取り上げられ，再生医療を一躍有名にした[1)]。その後，再生医療分野における研究は著しく発展し，ヒト胚性幹細胞（ES細胞），人工多能性幹細胞（iPS細胞）の樹立などが報告された。一方で，本邦で薬事承認を受けた再生医療製品は，現在のところ再生表皮のみであり，世界的に見ても，限局した軟骨欠損に対する再生軟骨が販売されているのみである。Tissue engineeringの提唱から20年を経てなお，実際の臨床で使用可能な再生医療製品の産業化が難航している現状を目の当たりにすると，再生医療の開発認可がいかに困難であるかが窺える。

顎顔面領域は四肢骨に比較して荷重負荷がかかりにくく，概して再建で必要とされる組織量も少ないことから，再生組織の移植に適した領域であると考えられる。とはいえ，既存の治療法である血管柄付骨移植，人工骨や人工歯根など様々な生体材料を用いた治療法，エピテーゼによる補綴などにより，形態的にも良好な組織再建が可能となってきている。従って，顎顔面領域における再生医療の展開は，既存の医療を低侵襲治療として凌駕する，或いは，より卓越した治療効果を発揮することにより可能になると考える。本稿では，われわれのグループが開発し実用段階に達している骨・軟骨再生医療について紹介する。

Ⅱ．In situ tissue engineering

下顎骨再建のfirst choiceとして用いられることが多い血管柄付遊離腓骨移植は，①血行が豊富な長い骨を採取できる，②インプラントを植立するのに十分な太さがある，③頭部操作と並行して，下肢から骨皮弁を採取できる，④皮膚欠損症例に対し，皮膚移植も同時に行える，⑤採取部の合併症が少ないことなどの特長を有している[2)]。しかし，健常部にメスを入れて採骨するために侵襲性は高く，採取できる骨の量と形状には大きな制約がある。また，移植部に適合した形状にするために，術中に移植骨の削合が必要となることが多い。

そこで近年注目を集めているのが，腸骨から採取

[1)] 東京大学医学部附属病院顎口腔外科・歯科矯正歯科
[2)] 東京大学大学院医学系研究科軟骨・骨再生医療寄付講座（富士ソフト）
[3)] 東京大学大学院工学系研究科バイオエンジニアリング専攻
［平成24年3月2日受付，平成24年5月18日受理］

した骨髄海綿骨（particulate cancellous bone and marrow: PCBM）とチタンメッシュトレーによる骨再建法である[3,4]。この方法では，トレーを適切に整形することにより，より自然な形態修復が可能であり，義歯やインプラントなどを併用した良好な咬合回復も期待できる。

PCBM移植では，PCBMに含まれる未分化間葉系由来の細胞による新生骨形成，それに引き続く骨吸収，骨形成により，周囲の母床骨に対応した骨改造が誘導される[5]。つまり，PCBM移植は，自己の骨形成能を利用した，いわゆるin situ tissue engineeringであり，その点において，移植骨そのものの生着を目的とする従来のブロック骨移植や血管柄付き骨移植と根本的に異なっている。また，小顎症の治療で選択される骨延長術も，骨切り部が治癒する過程で生じる仮骨をゆっくりと牽引することにより骨形成を誘導する治療法であり，PCBM移植と同様，in situ tissue engineeringに基づいた治療法であるといえる。このように，再生医療は必ずしも目新しい治療というわけではなく，従来から行われている治療にも，再生医療の概念を利用した治療法が見受けられる。

PCBMとチタンメッシュトレーを用いた手術法の課題として，術後感染の合併があげられる。オトガイ部や下顎枝などを含む再建では，複雑な形態のためトレーの整形が困難であり，皮膚や粘膜の裂開，死腔を生じやすいためであると推察される[4]。将来的には，術前の3Dモデルなどからカスタムメイドのメッシュトレーを作製し，より精度の高い再建を行うことにより安定した治療成績を維持することが可能になると思われる。

Ⅲ．骨再生医療（CT bone）

従来のブロック骨移植や血管柄付き骨移植は，患者自身の健常部から採取するため，移植後の骨癒合も良好で，修復効果も高い。また，チタンメッシュトレーとPCBMを利用した顎骨再建術は，tissue engineeringの概念を利用した骨再生法であり，従来の骨移植法と比較しても多くの利点を有している。しかし，いずれの方法も，自家骨移植であるため採骨部への侵襲は避けられず，採取量にも限界がある。諸外国では，他家骨移植という選択肢もあるが，本邦では，文化的・制度的な背景から普及していない。そこでわれわれは，形状，強度に優れ，且つ分解吸収性がよく，将来的には自己の骨に置換するような人工骨の開発に取り組んできた。

現在，人工骨の主流は，リン酸カルシウムのブロック状多孔体，ペースト，顆粒などである。リン酸カルシウムが頻用される理由としては，骨の一成分であるため生体適合性，生体安全性に優れていること，また，石灰岩とリン鉱石から合成されるため，供給量に制限がないことなどがあげられる[6]。しかし，現段階の人工骨は，強度，形状，操作性，分解吸収・再生誘導能などの機能面において自家骨や他家骨には及ばず，これらの課題を克服する新たな人工骨の開発が求められている。

われわれは，東京大学大学院工学系研究科と連携し，三次元インクジェットプリンターを用いたリン酸三カルシウム粉体積層造形法によるカスタムメイド人工骨（CT bone）の作製を検討してきた[7]。この方法では，リン酸三カルシウム粉体の薄層（0.1 mm）を作り，その上から水を主体とする硬化液をプリントするという過程を繰り返すことにより，外部形状のみならず，内部構造も自由に制御可能な人工骨を作製することができる。大型実験動物を用いた前臨床研究を経て，先天異常，外傷，腫瘍切除などにより非荷重部位に顎顔面変形を有する患者を対象に2006年3月から7月に臨床研究を10例，2008年10月から2009年9月に治験を10例行った（図1）[8]。患者のCT画像をもとに人工骨を作製するため，患部への適合も良好で，術者による形状調整がほぼ不要であった。また，十分な強度を有するため，優れた操作性を示すことも明らかとなった。これまでのところ安全面での問題はなく，人工骨と母骨との癒合も速やかに起こっていることが確認されている。

今後は荷重部への適応拡大を目指し，金属など他材料とのハイブリッド化や骨誘導シグナルとの融合などによる高機能化人工骨の開発が期待される。

Ⅳ．軟骨再生医療（インプラント型再生軟骨）

一般に，軟骨組織は自己修復能に乏しく，いったん障害を受けると自然回復は望めない。従って，関節軟骨損傷などの外傷や変形性関節症などの加齢性疾患，関節リウマチなどの炎症性疾患を患うと，歩行などの生活動作に支障をきたすこととなる。治療としては，人工関節置換術や自家軟骨移植などが行われているが，耐久性，感染，採取部位の侵襲などの課題があり，軟骨再生医療の開発に期待が寄せられている。

軟骨再生医療は，皮膚や角膜などとともに再生医療のなかでも比較的臨床応用が進んでいる分野である。関節軟骨の局所的な欠損に対しては，非荷重部の関節軟骨から軟骨細胞を単離し，培養増殖させた後に細胞懸濁液として欠損部に投与する自家軟骨細胞移植（autologous chondrocyte implantation: ACI）

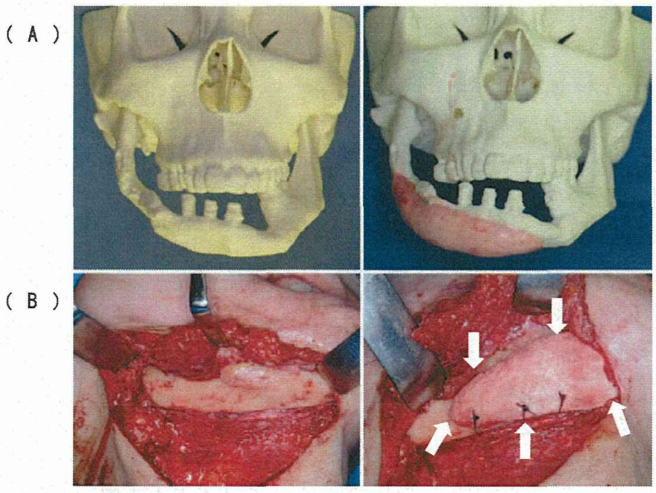

図 1　カスタムメイド人工骨（CT bone）
30 歳女性。下顎再建後の下顎変形に対し，リン酸三カルシウム粉体積層造形法により作製した CT bone を移植した。
（A）三次元造形モデルを利用した CT bone のデザイン
（B）右側下顎欠損部の陥凹部に移植された CT bone（矢印）。固定は吸収糸を用いて行った。

が，欧米を中心に医療として普及している[9]。しかしその適応範囲は依然として限局的で，層剥離，骨膜パッチの肥厚やグラフト逸脱などの問題点も指摘されている。また，既存の治療法と比較した際に，明らかな臨床上の優位性が認められないなど治療成績の限界も報告されている。顎顔面領域においても，隆鼻術後のシリコンインプラント抜去例や鞍鼻などに対して，患者の軟骨組織から単離した軟骨細胞を増殖培養させた後，皮下ポケットなどに注入して皮下再生軟骨を得るという方法が報告されている[10]。

このように，現行の軟骨再生医療は局所的な軟骨欠損の補填を目的とするため，移植される細胞は液状あるいはゲル状であり，膝関節の荷重に十分耐えうるような，あるいは顎顔面領域に適応可能な三次元形状を有する軟骨組織の再生は望めない。従って，軟骨再生医療の適応を，重度な軟骨損傷を伴う変形性関節症や顎顔面領域の先天性形態異常などへ拡大していくためには，力学的強度と適切な三次元形状を有する再生軟骨の開発が必要となる。そこでわれわれは，再生医療の 3 要素，すなわち細胞，成長因子，足場の観点から詳細な検討をすすめ，口唇口蓋裂に伴う重度の鼻変形（唇裂鼻変形）に適応可能なインプラント型再生軟骨の開発に取り組んできた。

細胞としては，軟骨組織由来の軟骨細胞，組織幹細胞に分類される種々の細胞のほか，胎生幹細胞（ES 細胞）あるいは人工多能性幹細胞（iPS 細胞）などが候補となりうる。このうち，①細胞培養により旺盛に増殖する[11]，②移植後自然に成熟する，③免疫拒絶や癌化のリスクが低い，④採取が比較的容易である，⑤倫理的に特に問題とならない，という特性を有する自家耳介軟骨細胞の活用が実用的であると判断した。成長因子に関しては，医薬品として既に安全性が確立されている 12 種類の成長因子・ホルモン（FGF-2，IGF-I，insulin，BMP-2 など）の組み合わせを，統計学的手法 fractional factorial design を用いて最適化し，ヒト軟骨細胞を 3 週間で 1000 倍程度増殖させる増殖培養液を開発した（ヒト血清および FGF-2/insulin 含有培養液 HFI）[12]。また，足場には，医療用生分解性ポリマーとして既に臨床応用されているポリ乳酸（poly-L-lactic acid:

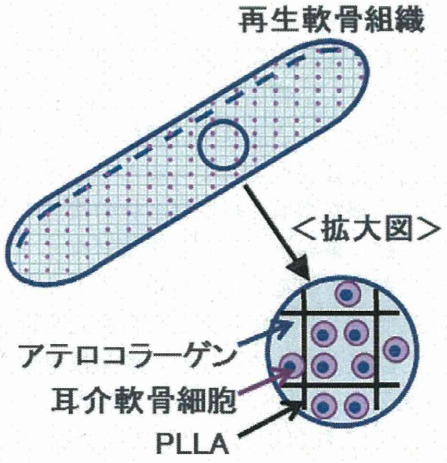

図 2　インプラント型再生軟骨

PLLA）やポリグリコール酸（poly-glycol acid: PGA）に関して形状検討を行い，アテロコラーゲンゲルとPLLA多孔体を組み合わせた足場素材複合体を開発した[13,14]。これらの知見を組み合わせることにより，生理的軟骨組織に匹敵する力学的強度を有するインプラント型再生軟骨の作製に成功した（図2）。大型動物を用いた前臨床試験において有効性と安全性を確認し，厚生労働省「ヒト幹細胞を用いる臨床研究に関する指針」に基づいて，学内臨床研究審査員会および厚生科学審議会の審議を経て，平成23年3月に厚生労働大臣の同意ならびに機関承認を受けた。現在，口唇鼻変形患者に対し，インプラント型再生軟骨の自主臨床研究を行っている（予定症例数3）。

V．将来展望

われわれが開発に携わってきた骨軟骨再生医療も，ようやく臨床応用段階に入ってきた。今後さらに汎用化，産業化を促し，再生医療を一層躍進させるためには，細胞培養に伴う複雑な製造工程を単純化することが望ましい。とはいえ，自己修復力に乏しい軟骨組織，関節組織の修復・再建，あるいは自然修復が困難な大型骨欠損に対しては，細胞を投与しなければ治癒は見込まれず，組織再生・再建のための細胞投与は必要不可欠であると考える。そこでわれわれは，細胞増殖と組織複合化の機能を再生組織の足場素材に集約・内蔵し，細胞プロセッシングセンターにおける製造工程を再現するような仕組みを再生組織そのものに組み込む技術開発を行っている（独立行政法人新エネルギー・産業技術総合開発機構　健康安心イノベーションプログラム，平成22-26年度）。これにより，再生医療製品に伴う複雑な製造工程の簡素化や培養期間の短縮化が実現すれば，品質の安定化と製品の普及に繋がるため，再生医療の新たな時代を築くことができるのではないかと期待している。

文　献

1) Langer R, Vacanti JP: Tissue engineering. Science 260：920-926, 1993.
2) 森　良之，高戸　毅：下顎再建における骨延長術の応用．口腔腫瘍，22：145-148，2010.
3) Iino M, Fukuda M, Nagai H, et al: Evaluation of 15 mandibular reconstructions with Dumbach Titan Mesh-System and particulate cancellous bone and marrow harvested from bilateral posterior ilia. Oral Surg Oral Med Oral Pathol Oral Radiol Endod 107：e1-8, 2009.
4) 飯野光喜，森　良之，近津大地，他：再生医学のいま　基礎研究から臨床への展開に向けて　In vivo tissue engineeringによる下顎骨再建．治療，91：2311-2315，2009.
5) 飯野光喜，森　良之，近津大地，他：【骨・軟骨の再生医療UPDATE】In vivo tissue engineeringによる顎骨再建の実際．Clinical Calcium，18：1757-1766，2008.
6) 鄭　雄一：インクジェットプリンターによるカスタムメイド人工骨．内分泌・糖尿病・代謝内科，32：305-310，2011.
7) 井川和代，望月　学，杉森　理，他：三次元インクジェットプリンターにより直接的に組み立てたテーラーメイドリン酸三カルシウム骨インプラント．人工臓器，37：14-16，2008.
8) Saijo H, ChungUng-Il, Igawa K, et al: 顎顔面における人工骨の臨床応用．J Artifi Org　11：171-176, 2008.
9) Marlovits S, Trattnig S: Cartilage repair. Eur J Radiol　57：1-2, 2006.
10) Yanaga H, Yanaga K, Imai K, et al: Clinical application of cultured autologous human auricular chondrocytes with autologous serum for craniofacial or nasal augmentation and repair. Plast Reconstr Surg 117：2019-2030, 2006.
11) Asawa Y, Ogasawara T, Takahashi T, et al: Aptitude of auricular and nasoseptal chondrocytes cultured under a monolayer or three-dimensional condition for cartilage tissue engineering. Tissue Eng Part A　15：1109-1118, 2009.
12) Takahashi T, Ogasawara T, Asawa Y, et al: Three-dimensional microenvironments retain chondrocyte phenotypes during proliferation culture. Tissue Eng 13：1583-1592, 2007.
13) Yamaoka H, Tanaka Y, Nishizawa S, et al: The application of atelocollagen gel in combination with porous scaffolds for cartilage tissue engineering and its suitable conditions. J Biomed Mater Res A　93：123-132, 2011.
14) Tanaka Y, Yamaoka H, Nishizawa S, et al: The optimization of porous polymeric scaffolds for chondrocyte/atelocollagen based tissue-engineered cartilage. Biomaterials　31：4506-4516, 2011.

Magn Reson Med Sci, Vol. 11, No. 1, pp. 27-34, 2012

MAJOR PAPER

Effects of Image Distortion Correction on Voxel-based Morphometry

Masami GOTO[1,2*], Osamu ABE[3], Hiroyuki KABASAWA[4], Hidemasa TAKAO[5], Tosiaki MIYATI[2], Naoto HAYASHI[6], Tomomi KUROSU[1], Takeshi IWATSUBO[7], Fumio YAMASHITA[8], Hiroshi MATSUDA[9], Sachiko INANO[5], Harushi MORI[5], Akira KUNIMATSU[5], Shigeki AOKI[10], Kenji INO[1], Keiichi YANO[1], and Kuni OHTOMO[5]; Japanese Alzheimer's Disease Neuroimaging Initiative

Departments of [1]Radiological Technology, [5]Radiology, and [6]Computational Diagnostic Radiology and Preventive Medicine, University of Tokyo Hospital
7-3-1 Hongo, Bunkyo-ku, Tokyo 113-8655, Japan
[2]Graduate School of Medical Science, Kanazawa University
[3]Department of Radiology, Nihon University School of Medicine
[4]Japan Applied Science Laboratory, GE Healthcare
[7]Department of Neuropathology, University of Tokyo
[8]Department of Radiology, National Center Hospital of Neurology and Psychiatry
[9]Department of Nuclear Medicine, Saitama Medical University International Medical Center
[10]Department of Radiology, Juntendo University
(Received April 27, 2011; Accepted August 31, 2011)

Purpose: We aimed to show that correcting image distortion significantly affects brain volumetry using voxel-based morphometry (VBM) and to assess whether the processing of distortion correction reduces system dependency.

Materials and Methods: We obtained contiguous sagittal T_1-weighted images of the brain from 22 healthy participants using 1.5- and 3-tesla magnetic resonance (MR) scanners, preprocessed images using Statistical Parametric Mapping 5, and tested the relation between distortion correction and brain volume using VBM.

Results: Local brain volume significantly increased or decreased on corrected images compared with uncorrected images. In addition, the method used to correct image distortion for gradient nonlinearity produced fewer volumetric errors from MR system variation.

Conclusion: This is the first VBM study to show more precise volumetry using VBM with corrected images. These results indicate that multi-scanner or multi-site imaging trials require correction for distortion induced by gradient nonlinearity.

Keywords: ***brain volumetry, distortion correction, gradient field nonlinearities, magnetic resonance imaging, voxel-based morphometry***

Introduction

Voxel-based morphometry (VBM)[1] using 3-dimensional T_1-weighted (3D-T_1) magnetic resonance (MR) images has been employed to estimate local brain volume.[2-5] Previous studies investigated whether distortion might cause error in estimating brain volume and evaluated the accuracy of various methods for correcting distortion.[6-8] However, those reports did not investigate the effect of distortion correction with regard to computational brain volumetry analyses (i.e., boundary shift integral,[9] VBM,[1] tensor-based morphometry,[10] and atlas-based volumetry[11]). We agree that use of images corrected for distortion improves analysis but believe additional study is required of VBM that includes spatial normalization. This study has 2 aims. The first is to show that correcting distortion significantly affects brain volumetry using VBM. Because analytical procedures that include normalization may reduce the influence of distortion correction in VBM and obscure the effects of correction, it is important to confirm the need for correction in

*Corresponding author, Phone: +81-3-3815-5411, Fax: +81-4-7183-3337, E-mail: car6_pa2_rw@yahoo.co.jp

VBM. Following distortion correction, regions of increased volume would correspond to regions of reduced volume caused by distortion, and regions of reduced volume would correspond to those with increased volume caused by distortion.

Our second aim is to assess whether system dependency decreases in the processing of distortion correction. In multi-site studies, data obtained using different MR imaging systems are mixed in the same analytical flow. Consequently, previous reports of multi-site studies[12–14] showed less precise brain volumetry as a result of heterogeneous signal intensity and low signal-to-noise ratio (SNR). The degree of image distortion depends on such variables within the MR imaging system.[15] However, no reports have shown reduced volumetric precision of VBM as a result of using distorted images.

Materials and Methods

Subjects

Twenty-two healthy volunteers (17 men, 5 women; aged 23 to 47 years, mean age 31.1 ± 7.3 years) underwent MR imaging at 1.5 and 3 tesla, with 3D-T_1 images obtained the same day. A board-certified radiologist (O.A.) inspected the images and found none of the following in any subject: brain tumor, infarction, hemorrhage, brain atrophy, cognitive impairment, or white matter lesions graded higher than grade 2 of Fazekas classification.[16] Cognitive impairment was screened with a mini-mental state examination, and T_2-weighted images were used to evaluate white matter lesions. The ethical committee of our institution approved the study, and written informed consent was obtained from all participants.

MR imaging protocol

We obtained MR imaging data using 2 systems. The first was a 1.5T scanner (Signa EXCITE HD, GE Healthcare, Waukesha, WI, USA; 33 mT/m maximum strength, 120 T/m/s slew rate) with a quadrature head coil used for transmission and reception. We used 3D magnetization-prepared rapid gradient-echo (3D-MPRAGE) to obtain 184 contiguous sagittal T_1-weighted images with slice thickness, 1.3 mm; repetition time (TR)/echo time (TE), 3000 ms/3.9 ms; inversion time (TI), 1000 ms; flip angle, 8°; field of view (FOV), 24 cm; number of excitations (NEX), one; and matrix, 192 × 192 pixels. We used 2D fast spin-echo (2D-FSE) to obtain 48 axial T_2-weighted images with slice thickness, 3 mm; TR/TE, 3000 ms/100 ms; echo train length, 16; FOV, 24 cm; NEX, one; and matrix, 256 × 256 pixels.

The second system was a 3T scanner (Signa EXCITE HDx, GE Healthcare; 40 mT/m maximum strength, 150 T/m/s slew rate) with a quadrature head coil used for transmission and reception. We used 3D-MPRAGE to obtain 170 contiguous sagittal T_1-weighted images with slice thickness, 1.3 mm; TR/TE, 2300 ms/2.8 ms; TI, 900 ms; flip angle, 8°; FOV, 26 cm; NEX, one; and matrix 256 × 256 pixels. We used 2D-FSE to obtain 48 axial T_2-weighted images with slice thickness, 3 mm; TR/TE, 3000 ms/97 ms; echo train length, 16; FOV, 24 cm: NEX, one; and matrix, 256 × 256 pixels. We employed scanning protocols using the protocol of the Alzheimer's Disease Neuroimaging Initiative.

Image preprocessing for VBM

We used Statistical Parametric Mapping 5 (SPM5)[17] software for volumetric analysis, nonparametric nonuniform intensity normalization (N3) software[18] for intensity bias correction, and spherical harmonics description of gradients (SHDG)[8] for gradient nonlinearity distortion correction. Image distortion in MR has 6 potential sources–scale errors (linear) in gradient fields, shimming anomalies of the main magnet, chemical shift, B_0 eddy currents, nonlinearities of gradient fields, and magnetic susceptibility variations in various anatomical structures.[19] We can correct nonlinearities of gradient fields and know their influence is large, but we cannot correct magnetic susceptibility variations in anatomical structures. Therefore, we focused only on image distortion caused by nonlinearities of gradient fields.

The various distortion correction methods include SHDG, phase mapping,[20] adoption of a specially constructed phantom,[21] and the use of 2 frequency-encoding gradients.[22] We employed SHDG correction for nonlinearities of the gradient fields using the same method described by Jovicich and colleagues,[8] which employs information based on the design of the gradient coils; we used MR-specific information, such as the gradient correction coefficients. SHDG correction can correct image distortion caused by nonlinearities of the gradient fields but not distortion caused by other factors, such as magnetic susceptibility variations in various anatomical structures. Jovicich's group[8] reported the efficiency of SHDG correction in a study that showed distorted areas using a grid phantom and differences in brain surface boundaries using images of the human brain. Therefore, we further evaluated this method for VBM that included normalization.

We processed 3D-MPRAGE images with and without SHDG correction in SPM5 after N3 proc-

essing. In SPM5, 3D-MPRAGE images in native space were bias-corrected, spatially normalized, and segmented into images (i.e., gray matter, white matter, and cerebrospinal fluid); voxel size of the spatially normalized images was $2\times2\times2$ mm. We changed the affine regularization space template in the International Consortium for Brain Mapping from the European to the East Asian brain template. In the modulation step, we multiplied the voxel values of the spatially normalized gray and white matter images by a measure of the relative volumes of the warped and unwarped structures that were derived from the nonlinear step of spatial normalization (Jacobian determinant).

For each subject, we added the spatially normalized image of gray matter and that of white matter and defined this as the brain image in this study. Spatially normalized brain images were smoothed with 8-mm isotropic Gaussian kernels. Four sets of each processed volume were obtained as follows: (A) brain images with SHDG correction obtained with the 1.5T system; (B) brain images without SHDG correction obtained with the 1.5T system; (C) brain images with SHDG correction obtained with the 3T system; and (D) brain images without SHDG correction obtained with the 3T system.

To test for a statistically significant effect of distortion correction, we prepared differential images (DI). DI-1.5 was defined as (brain image with SHDG correction obtained with the 1.5T system) − (brain image without SHDG correction obtained with the 1.5T system). In statistical analysis of DI-1.5 for the 22 subjects, we assessed the effect of SHDG correction.

To investigate reduction in system dependency, we prepared DI-C and DI-nonC: DI-C was defined as (brain image with SHDG correction obtained with the 1.5T system) − (brain image with SHDG correction obtained with the 3T system), and DI-nonC was defined as (brain image without SHDG correction obtained with the 1.5T system) − (brain image without SHDG correction obtained with the 3T system). In statistical analysis of DI-Cs and DI-nonCs of the 22 subjects, we assessed whether SHDG correction resulted in fewer volumetric errors caused by variation in MR system.

Statistical analyses for the effect of distortion correction

We compared estimated brain volumes with and without SHDG correction using the DI-1.5s of the 22 subjects and analyzed the DI-1.5s with SPM5, employing the framework of the general linear model. To test hypotheses with respect to regionally specific group effects, we tested the estimates with one-sample t-test using VBM. In this analysis, "plus regions" were regions increased by SHDG correction, and "minus regions" were regions reduced by SHDG correction. The significance of each region was estimated by distributional approximations from the random Gaussian fields theory. $P<0.05$, corrected with family-wise error (FWE) in voxel difference and cluster size greater than 30 voxels, was considered statistically significant.

Statistical analyses for reduction of system dependency

We examined whether SHDG correction could reduce brain volumetric errors caused by MR system variation. We analyzed the DI-Cs and DI-nonCs of the 22 subjects using SPM5, employing the framework of the general linear model. To test hypotheses with respect to regionally specific group effects, we compared estimates with 2 linear contrasts using VBM. Correction of image distortion by SHDG indicated significant difference between DI-C and DI-nonC. The significance of each region was estimated by distributional approximations from the theory of random Gaussian fields. $P<0.05$, corrected with FWE in voxel difference and cluster size greater than 30 voxels, was considered statistically significant.

We prepared 2 design matrices to estimate system dependence in regions increased or reduced by nonlinearities of gradient fields. We used the first matrix (Fig. 3) to investigate system dependence inside regions reduced by SHDG correction. In analysis using this matrix, we estimated significant minus regions in the DI-nonC of the 22 subjects by VBM (uncorrected $P<0.05$) and set these minus regions as an inclusive mask. These significant minus regions indicated that volume expansion caused by nonlinearities of gradient fields was greater in the 3T system than the 1.5T system.

We used the second matrix (Fig. 4) to investigate system dependence within regions increased by SHDG correction. In analysis using this matrix, we estimated significant plus regions in the DI-nonC of the 22 subjects by VBM (uncorrected $P<0.05$) and set these plus regions as an inclusive mask. These significant plus regions indicate that volume reduction caused by nonlinearities of gradient fields was greater in the 3T system than the 1.5T system.

Results

Results of comparison between images with and without SHDG correction

Various regions of the brain showed significantly reduced (Fig. 1) and increased (Fig. 2) volumes fol-

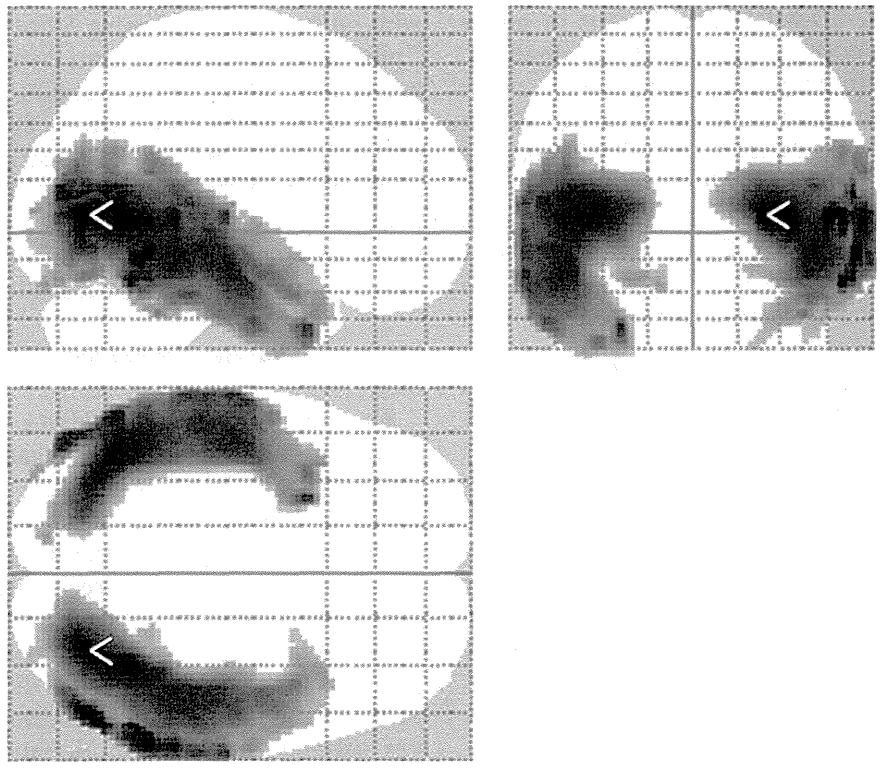

Fig. 1. The figure is a "glass brain" that indicates all regions in which brain volume was significantly reduced on corrected images compared to those without correction (gray scale, voxel with maximum effect indicated by red pointer). $P<0.05$, corrected with family-wise error (FWE) in voxel difference and cluster size greater than 30 voxels, was considered statistically significant.

lowing SHDG correction. Figure 1 shows all regions in which corrected images demonstrated significantly reduced local brain volume compared with uncorrected images. The Montreal Neurological Institute (MNI) coordinates of local maxima were 28, −70, 6 ($P<0.001$, T value = 14.97, cluster size = 12597). Figure 2 shows all regions in which corrected images demonstrated significantly increased local brain volume compared uncorrected images. MNI coordinates of local maxima were 22, 4, 54 ($P<0.001$, T value = 21.61, cluster size = 24441).

Results of brain volumetry error caused by MR system variation

SHDG correction decreased the system dependence of estimated brain volumes. Figure 3 shows all regions in which DI-nonC using uncorrected images had significant minus regions in comparison with DI-C using corrected images. In other words, brain volumetry was more system dependent using uncorrected images than corrected images; SHDG correction decreased system dependence within regions reduced by correction. MNI coordinates of local maxima were −46, −28, −12 ($P<0.001$, T value = 12.38, cluster size = 5573). Figure 4 shows all regions in which the DI-nonC of uncorrected images demonstrated significant plus regions in comparison with the DI-C of corrected images. In other words, brain volumetry was more system dependent using uncorrected images than corrected images; SHDG correction reduced system dependence within regions increased by correction. MNI coordinates of local maxima were −18, −8, 50 ($P<0.001$, T value = 10.07, cluster size = 7727). Figure 5 shows T_1WI with and without SHDG correction for a single subject.

Discussion

In our VBM study, we detected areas whose volumes increased or reduced by image distortion caused by nonlinearities of the gradient fields. Volume was reduced in the area around the temporal lobe and increased in the area around the frontal and parietal lobes. Thus, the influence of image distortion extends to the deep regions of the brain as well as surface regions. The results of com-

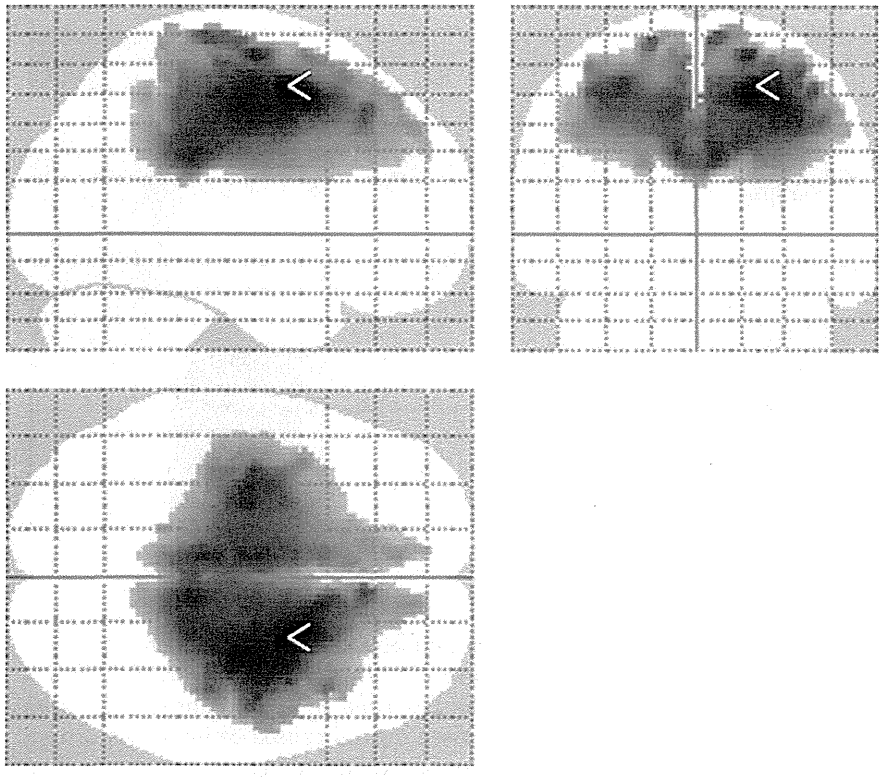

Fig. 2. The figure is a "glass brain" that indicates all regions in which brain volume was significantly increased on corrected images compared to those without correction (gray scale, voxel with maximum effect indicated by red pointer). $P<0.05$, corrected with family-wise error (FWE) in voxel difference and cluster size greater than 30 voxels, was considered statistically significant.

parison between corrected and uncorrected images (Figs. 1, 2) seem to deviate from the orthogonal frame of the gradients because the axis of the figures deviates from that frame; the images were obtained with most subjects lifting their chins against that frame. Therefore, we think that the areas of significant difference in our results are distributed according to the orthogonal frame of the gradients. The present study is the first to clarify the effect of SHDG correction on VBM.

McRobbie and associates showed that the amount of image distortion differs for each system.[15] Because distortion influences the results of VBM analysis, we considered the distortion to be related to system dependence. Therefore, we assessed whether image distortion correction processing resulted in reduced system dependency. The results (Figs. 3, 4) showed that SHDG correction reduced system dependency. Unfortunately, this result does not prove that distortion correction completely eliminates system dependency, but it does provide insight into the need for correcting image distortion in multi-site studies. Even in a study using a single system, image distortion affects analytical results because spatial placement of the main magnetic field center and the brain center influences the deformation volume due to distortion. This spatial placement in imaging differs among subjects.[8] In addition, the use of image distortion correction is strongly recommended in multi-site studies to minimize volumetric errors caused by system variation. In many institutions, however, VBM researchers may not always have access to MR-specific information or vendor-specific technical information, such as the gradient correction coefficients that should be used to perform SHDG correction. Therefore, previous studies may have utilized VBM studies using uncorrected images.

The major limitation of our study is that we cannot know the true brain volume. Neither can we explain whether the SHDG method performed excessive correction in this study. Therefore, we could demonstrate only that in brain volumetry using VBM, volume differed between SHDG-corrected and noncorrected images, and volumetry error due to system variation was decreased when image distortion correction was employed. Unfortunately, we could not show that VBM analysis with distor-

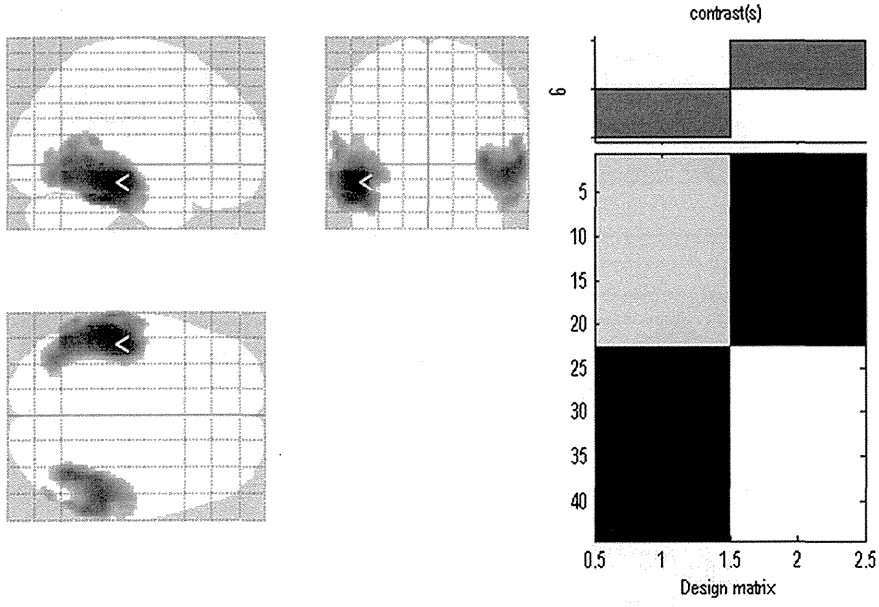

Fig. 3. Left side, a "glass brain" that indicates all regions in which system dependence was significantly less in corrected images than uncorrected images (gray scale, voxel with maximum effect indicated by red pointer). This figure showed system dependence inside increased regions caused by image distortion. Right side, design matrix. The left group in the design matrix comprised differential images (DI)-nonC and the right group, DI-C. P value < 0.05, uncorrected in voxel difference and cluster size greater than 30 voxels, was considered statistically significant.

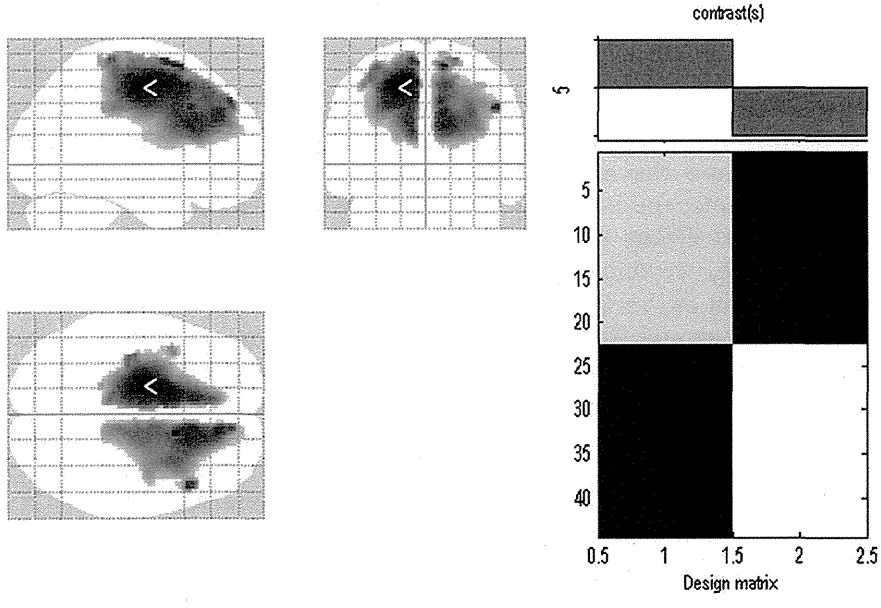

Fig. 4. Left side, a "glass brain" that indicates all regions in which system dependence was significantly less in corrected images than uncorrected images (gray scale, voxel with maximum effect indicated by red pointer). This figure showed system dependence inside reduced regions caused by image distortion. Right side, design matrix. The left group in the design matrix comprised differential images without correction (DI-nonC) and the right group, those with correction (DI-C). $P < 0.05$, uncorrected in voxel difference and cluster size greater than 30 voxels, was considered statistically significant.

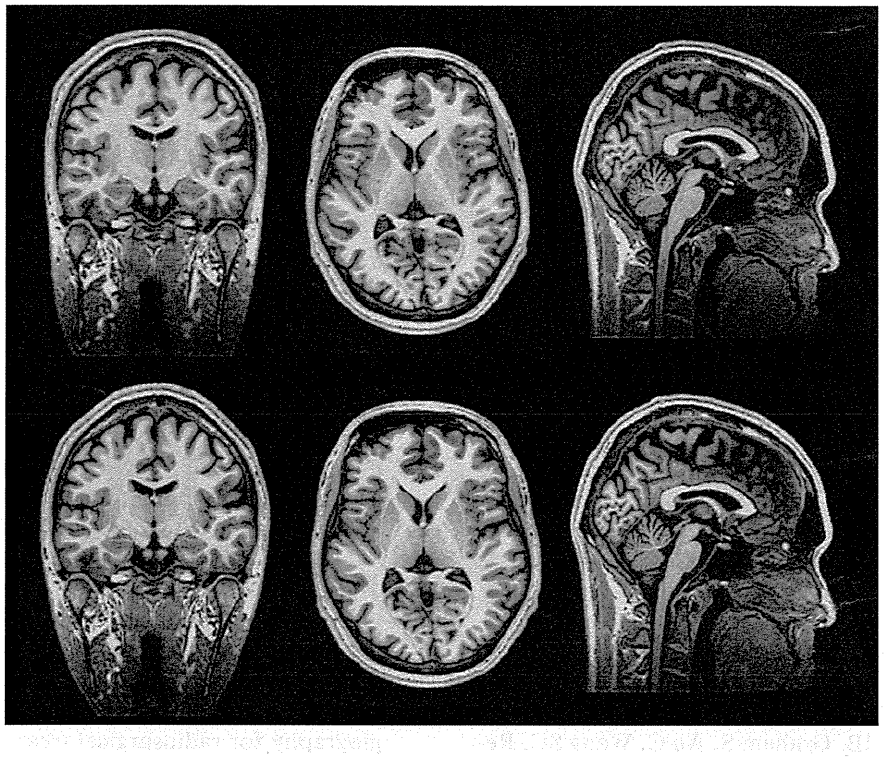

Fig. 5. Upper side, T_1W-weighted imaging (T_1WI) with spherical harmonics description of gradients (SHDG) correction; lower side, T_1WI without SHDG correction of a subject in the present study. Figure shows representative coronal, axial, and saggital slices of the original structural T_1 volume.

tion correction more accurately estimated brain volume. However, in their phantom study, Jovicich's group showed that the phantom volume from a corrected image was much closer to the true phantom volume.[8] We performed a similar inspection and obtained a similar result. Therefore, we can conclude that VBM analysis using a corrected image provides a result near to the true brain volume.

Conclusions

We believe this is the first VBM study to show that the use of corrected images can reduce volumetric errors caused by system variations. These results indicate that correction of distortion induced by gradient nonlinearity is mandatory in multi-scanner or multi-site imaging trials.

Acknowledgments

This study was supported by grants-in-aid for Comprehensive Research on Aging and Health from the Ministry of Health, Labor and Welfare, Japan.

References

1. Ashburner J, Friston KJ. Voxel-based morphometry—the methods. Neuroimage 2000; 11:805–821.
2. Good CD, Johnsrude I, Ashburner J, Henson RN, Friston KJ, Frackowiak RS. Cerebral asymmetry and the effects of sex and handedness on brain structure: a voxel-based morphometric analysis of 465 normal adult human brains. Neuroimage 2001; 14:685–700.
3. Nunnemann S, Wohlschläger AM, Ilg R, et al. Accelerated aging of the putamen in men but not in women. Neurobiol Aging 2009; 30:147–151.
4. Sato K, Taki Y, Fukuda H, Kawashima R. Neuroanatomical database of normal Japanese brains. Neural Netw 2003; 16:1301–1310.
5. Draganski B, Gaser C, Busch V, Schuierer G, Bogdahn U, May A. Neuroplasticity: changes in grey matter induced by training. Nature 2004; 427: 311–312.
6. Doran SJ, Charles-Edwards L, Reinsberg SA, Leach MO. A complete distortion correction for MR images: I. Gradient warp correction. Phys Med Biol 2005; 50:1343–1361.
7. Janke A, Zhao H, Cowin GJ, Galloway GJ, Doddrell DM. Use of spherical harmonic deconvolu-

tion methods to compensate for nonlinear gradient effects on MRI images. Magn Reson Med 2004; 52:115–122.
8. Jovicich J, Czanner S, Greve D, et al. Reliability in multi-site structural MRI studies: effects of gradient non-linearity correction on phantom and human data. Neuroimage 2006; 30:436–443.
9. Barnes J, Scahill RI, Boyes RG, et al. Differentiating AD from aging using semiautomated measurement of hippocampal atrophy rates. Neuroimage 2004; 23:574–581.
10. Thompson PM, Giedd JN, Woods RP, MacDonald D, Evans AC, Toga AW. Growth patterns in the developing brain detected by using continuum mechanical tensor maps. Nature 2000; 404: 190–193.
11. Gonoi W, Abe O, Yamasue H, et al. Age-related changes in regional brain volume evaluated by atlas-based method. Neuroradiology 2010; 52:865–873.
12. Leow AD, Klunder AD, Jack CR Jr., et al. Longitudinal stability of MRI for mapping brain change using tensor-based morphometry. Neuroimage 2006; 31:627–640.
13. Shuter B, Yeh IB, Graham S, Au C, Wang SC. Reproducibility of brain tissue volumes in longitudinal studies: effects of changes in signal-to-noise ratio and scanner software. Neuroimage 2008; 41: 371–379.
14. Han X, Jovicich J, Salat D, et al. Reliability of MRI-derived measurements of human cerebral cortical thickness: the effects of field strength, scanner upgrade and manufacturer. Neuroimage 2006; 32:180–194.
15. McRobbie DW, Quest RA. Effectiveness and relevance of MR acceptance testing: results of an 8 year audit. Br J Radiol 2002; 75:523–531.
16. Fazekas F, Chawluk JB, Alavi A, Hurtig HI, Zimmerman RA. MR signal abnormalities at 1.5T in Alzheimer's dementia and normal aging. AJR Am J Roentgenol 1987; 149:351–356.
17. Ashburner J, Friston KJ. Unified segmentation. Neuroimage 2005; 26:839–851.
18. Sled JG, Zijdenbos AP, Evans AC. A nonparametric method for automatic correction of intensity nonuniformity in MRI data. IEEE Trans Med Imaging 1998; 17:87–97.
19. Sumanaweera TS, Glover GH, Binford TO, Adler JR. MR susceptibility misregistration correction. IEEE Trans Med Imaging 1993; 12:251–259.
20. Sumanaweera TS, Glover GH, Hemler PF, et al. MR geometric distortion correction for improved frame-based stereotaxic target localization accuracy. Magn Reson Med 1995; 34:106–113.
21. Schad LR, Ehricke HH, Wowra B, et al. Correction of spatial distortion in magnetic resonance angiography for radiosurgical treatment planning of cerebral arteriovenous malformations. Magn Reson Imaging 1992; 10:609–621.
22. Chang TY, Hong JH, Yeh P. Spatial amplification: an image-processing technique using the selective amplification of spatial frequencies. Opt Lett 1990; 15:743–745.

Eur Radiol (2012) 22:1613–1623
DOI 10.1007/s00330-012-2452-z

COMPUTED TOMOGRAPHY

Model-based iterative reconstruction technique for radiation dose reduction in chest CT: comparison with the adaptive statistical iterative reconstruction technique

Masaki Katsura · Izuru Matsuda · Masaaki Akahane · Jiro Sato · Hiroyuki Akai · Koichiro Yasaka · Akira Kunimatsu · Kuni Ohtomo

Received: 22 December 2011 / Revised: 22 February 2012 / Accepted: 23 March 2012 / Published online: 27 April 2012

Abstract
Objectives To prospectively evaluate dose reduction and image quality characteristics of chest CT reconstructed with model-based iterative reconstruction (MBIR) compared with adaptive statistical iterative reconstruction (ASIR).
Methods One hundred patients underwent reference-dose and low-dose unenhanced chest CT with 64-row multidetector CT. Images were reconstructed with 50 % ASIR-filtered back projection blending (ASIR50) for reference-dose CT, and with ASIR50 and MBIR for low-dose CT. Two radiologists assessed the images in a blinded manner for subjective image noise, artefacts and diagnostic acceptability. Objective image noise was measured in the lung parenchyma. Data were analysed using the sign test and pair-wise Student's t-test.
Results Compared with reference-dose CT, there was a 79.0 % decrease in dose–length product with low-dose CT. Low-dose MBIR images had significantly lower objective image noise (16.93±3.00) than low-dose ASIR (49.24± 9.11, $P<0.01$) and reference-dose ASIR images (24.93± 4.65, $P<0.01$). Low-dose MBIR images were all diagnostically acceptable. Unique features of low-dose MBIR images included motion artefacts and pixellated blotchy appearances, which did not adversely affect diagnostic acceptability.
Conclusion Diagnostically acceptable chest CT images acquired with nearly 80 % less radiation can be obtained using MBIR. MBIR shows greater potential than ASIR for providing diagnostically acceptable low-dose CT images without severely compromising image quality.

M. Katsura (✉) · I. Matsuda · M. Akahane · J. Sato · H. Akai · K. Yasaka · A. Kunimatsu · K. Ohtomo
Department of Radiology, Graduate School of Medicine, The University of Tokyo,
7-3-1 Hongo,
Bunkyo-ku, Tokyo 113-8655, Japan
e-mail: mkatsura-tky@umin.ac.jp

Key Points
- *Model-based iterative reconstruction (MBIR) creates high-quality low-dose CT images.*
- *MBIR significantly improves image noise and artefacts over adaptive statistical iterative techniques.*
- *MBIR shows greater potential than ASIR for diagnostically acceptable low-dose CT.*
- *The prolonged processing time of MBIR may currently limit its routine use in clinical practice.*

Keywords Model-based iterative reconstruction · Adaptive statistical iterative reconstruction · Radiation dose reduction · Image noise · Spatial resolution

Abbreviations and acronyms

MBIR	Model-based iterative reconstruction
ASIR	Adaptive statistical iterative reconstruction
FBP	Filtered back projection
MTF	Modulation transfer function
ED	Effective dose

Introduction

There are increasing concerns about the magnitude of the radiation dose delivered in computed tomography (CT) and the potential increase in the incidence of radiation-induced carcinogenesis [1]. The estimated annual effective dose (ED) from medical radiation exposure per individual in the United States (US) population has increased about six-fold over the past quarter century (from 0.53 mSv in 1980 to 3.0 mSv in 2006) [2]. This dramatic increase is largely attributable to the rapid

and substantial rise in CT utilisation (from 3,000,000 studies in the US in 1980 to 70,000,000 studies in 2006) [3]. Despite several activities that have been conducted to monitor and reduce the radiation dose delivered to patients [3], the US per capita ED from CT examinations in 2006 increased to 1.47 mSv, amounting to almost one half of total medical exposure [4].

Several dose-reduction techniques, such as tube current modulation [5], reduced tube voltage [6], use of a higher pitch [7] and noise reduction filters [8], have been successfully implemented and have been shown to reduce radiation exposure. However, further reductions in radiation dose are hindered by increased image noise and degraded image quality, mainly as a result of limitations of the standard filtered back projection (FBP) reconstruction algorithm currently used on most CT systems. Use of an iterative reconstruction (IR) algorithm is an alternative image reconstruction technique. Unlike conventional FBP, which is based on simpler mathematical assumptions of the tomographic imaging system, IR generates a set of synthesised projections by accurately modelling the data collection process in CT. One of the first IR algorithms released for clinical use was the adaptive statistical iterative reconstruction (ASIR) algorithm (GE Healthcare, Waukasha, WI, USA). Previous phantom and clinical studies have shown that ASIR provides diagnostically acceptable images with a reduction in image noise for low-radiation dose CT compared with the FBP algorithm [9–18].

The recently developed model-based iterative reconstruction (MBIR) is a much more complex and advanced IR technique than ASIR [19, 20] (see Appendix 1). Phantom experiments have shown that MBIR provides a significant reduction in image noise and streak artefacts, a significant improvement in spatial resolution, and has the potential to allow further radiation dose reduction without compromising image quality [19]. However, few data are available on its effect on radiation dose reduction in patients, and there are no clinical studies to our knowledge that have directly compared MBIR with ASIR. The purpose of this study was to evaluate dose reduction and image quality characteristics of three different chest CT protocols in the same patients: low-dose CT reconstructed with MBIR, low-dose CT reconstructed with ASIR and reference-dose CT reconstructed with ASIR.

Materials and methods

This prospective clinical study was compliant with Health Insurance Portability and Accountability Act guidelines and was approved by the Human Research Committee of our Institutional Review Board.

Patients

The Radiology Information System was checked to identify patients scheduled for unenhanced standard-of-care clinical chest CT examinations (around 5–10 per day) at a single tertiary care centre. Inclusion criteria for the present study were the following: age ≥18 years, the patient was scheduled for unenhanced standard-of-care CT examination of the chest, the ability to give written informed consent, and the ability to hold one's breath and remain still for at least 10 s. Patients who were unable to provide written informed consent, follow verbal commands for breath holding or remain still for the duration of CT acquisition were excluded. Women who were pregnant or were trying to get pregnant were also excluded.

Each potential subject was given a detailed informed consent form written in simple language about the objective, method and risks of study participation. The study procedure, which involved an acquisition of reference-dose CT followed by low-dose CT (both discussed later in detail), was explained to the subjects. They were also informed that the sum of reference-dose and low-dose CT acquisition would not exceed the radiation dose for standard-of-care chest CT at our institution. The risks associated with study participation, particularly the possible influence on diagnostic performance, in which the reference dose in the present study was expected to be slightly lower compared to radiation doses for standard-of-care CT, were explained to the subjects in simple language. Subjects were also informed that they would not receive any remuneration or benefit from their participation in the study.

Between 1 July 2011 and 28 July 2011, 113 consecutive eligible patients were identified. Nine patients refused to participate in the study, and 104 gave informed consent to participation in the study. None withdrew from the study after signing the consent form. To understand the evaluation system, two thoracic radiologists (HA and IM, with 8 and 6 years of experience, respectively) were trained in the subjective grading of image quality using the images of 4 patients, who were selected from the 104 patients using a random number table, and subsequently eliminated from the rest of the analysis. Therefore, 100 patients were included in the final analysis. The body weight of each patient was recorded as well as other demographic information (summarised in Table 1).

CT data acquisition

Unenhanced chest CT for reference-dose CT followed by low-dose CT (discussed later) were acquired with a 64-row multidetector CT system (Discovery CT750 HD; GE Healthcare). All patients in the study were able to undergo chest CT in the supine position with both arms elevated and with a single breath-hold for each acquisition. In this

Table 1 Patient characteristics and CT parameters

Men/women	55/45
Age (years)	65.6±12.4
Body weight (kg)	58.0±13.0
Acquisition mode	Helical
Tube voltage (kVp)	120
Field of view (mm)	350*
Gantry rotation time (s)	0.5
Table speed (mm per gantry rotation)	39.37
Detector configuration (mm)	64×0.625
Reconstructed section thickness (mm)	0.625
Pitch	0.984:1

Data are mean±standard deviation for each value unless indicated otherwise. A field of view of 350 mm was typically set; however, it was adjusted according to patient size (*). The main clinical indications for chest CT were as follows: follow-up for a pulmonary nodule (n=23), abnormal chest radiograph (n=19), interstitial lung disease (n=17), staging or restaging of known or suspected malignancy (n=13), ground-glass opacity (n=7), nontuberculous mycobacterial disease (n=6), obstructive pulmonary disease (n=4), haemoptysis (n=3), pulmonary tuberculosis (n=2), sarcoidosis (n=2), mediastinal mass (n=2), hypersensitivity pneumonitis (n=1) and asbestosis (n=1)

prospective clinical study, reference- and low-dose CTs were acquired with minimal differences in data acquisition conditions (with the exception of radiation dose). For instance, to minimise the positional difference between the two acquisitions for each patient, the time between completion of the reference-dose CT and initiation of imaging for low-dose CT was kept to a minimum (about 10 s or less). To avoid contrast enhancement bias owing to the delay in imaging from the start of the injection, only unenhanced CT images were included in this study. Imaging parameters for both acquisitions were held constant with the exception of noise index (NI, discussed later) and are summarised in Table 1. For reconstructing both reference-dose and low-dose CT images, we used the chest kernel (a proprietary kernel of GE Healthcare), which is equivalent to the lung kernel for depiction of lung and equivalent to the soft-tissue kernel for depiction of mediastinal soft-tissue structures [21, 22].

Rationale for slice thickness

All images were reconstructed with axial slices 0.625 mm thick, which is standard in our institution for reading high-resolution CT of the chest. Images with increased slice thickness or coronal/sagittal reformats were not used for evaluation in this study for the following reasons. It is known that image noise is dependent on the reconstruction thickness, as thicker slice reconstructions are less noisy than thinner slice reconstructions. Generally, image noise is inversely proportional to the square root of the slice thickness (e.g. by increasing slice thickness from 0.625 mm to 2.5 mm=4×0.625, image noise should decrease by a factor of 1 divided by the square root of 4). However, our preliminary results of phantom experiments indicate that this does not necessarily apply to MBIR, and the relationship between image noise and slice thickness is different depending on the reconstruction algorithm (unpublished data). Furthermore, MBIR and ASIR behave differently in terms of image noise when reformatted into coronal and sagittal slices (also unpublished data). Therefore, to directly compare image quality characteristics, only 0.625-mm-thick axial slices were used in the present study.

Noise index setting

Both reference- and low-dose CT protocols involved the use of automatic tube current modulation (ATCM; Auto mA 3D; GE Healthcare). The operator-selected NI level modulates the tube current during gantry rotation to achieve a predicted average statistical noise level in the images of the specified reconstruction slice thickness requested. In this study, a fixed NI of 31.5 was used for reference-dose CT and of 70.44 was used for low-dose CT. Both NIs are the predicted noise level at a slice thickness of 0.625 mm. The rationale for the NI setting in the present study is described in Appendix 2.

Image reconstruction

Images for reference-dose CT were reconstructed with blending of 50 % filtered back projection and 50 % ASIR image data (ASIR50). A blending factor of 50 % was chosen based on the previous literature [16, 17] and recommendations from the vendor. Images for low-dose CT were reconstructed with ASIR50 and MBIR. Blending with FBP does not apply to MBIR, as it is a pure IR technique (see Appendix 1). Thus, three image data sets (reference-dose ASIR, low-dose ASIR and low-dose MBIR) were generated in each patient (Fig. 1). Each image data set was coded, patient information was removed and the data sets were randomised before blinded evaluation (Fig. 2).

Objective image quality

Objective measurements were performed for the image data sets of 100 patients (300 image sets) on a workstation (Centricity RA1000; GE Yokogawa Medical Systems) by a radiologist (MK) with 4 years of imaging experience. Circular regions of interest (ROI) were drawn in the descending thoracic aorta at the level of the carina (15–20 mm in diameter) for each image data set. Calcifications, soft plaques of the aortic wall and areas with prominent streak artefacts were carefully avoided. Circular ROIs were also drawn in the homogeneous part of the lung parenchyma at the level of the

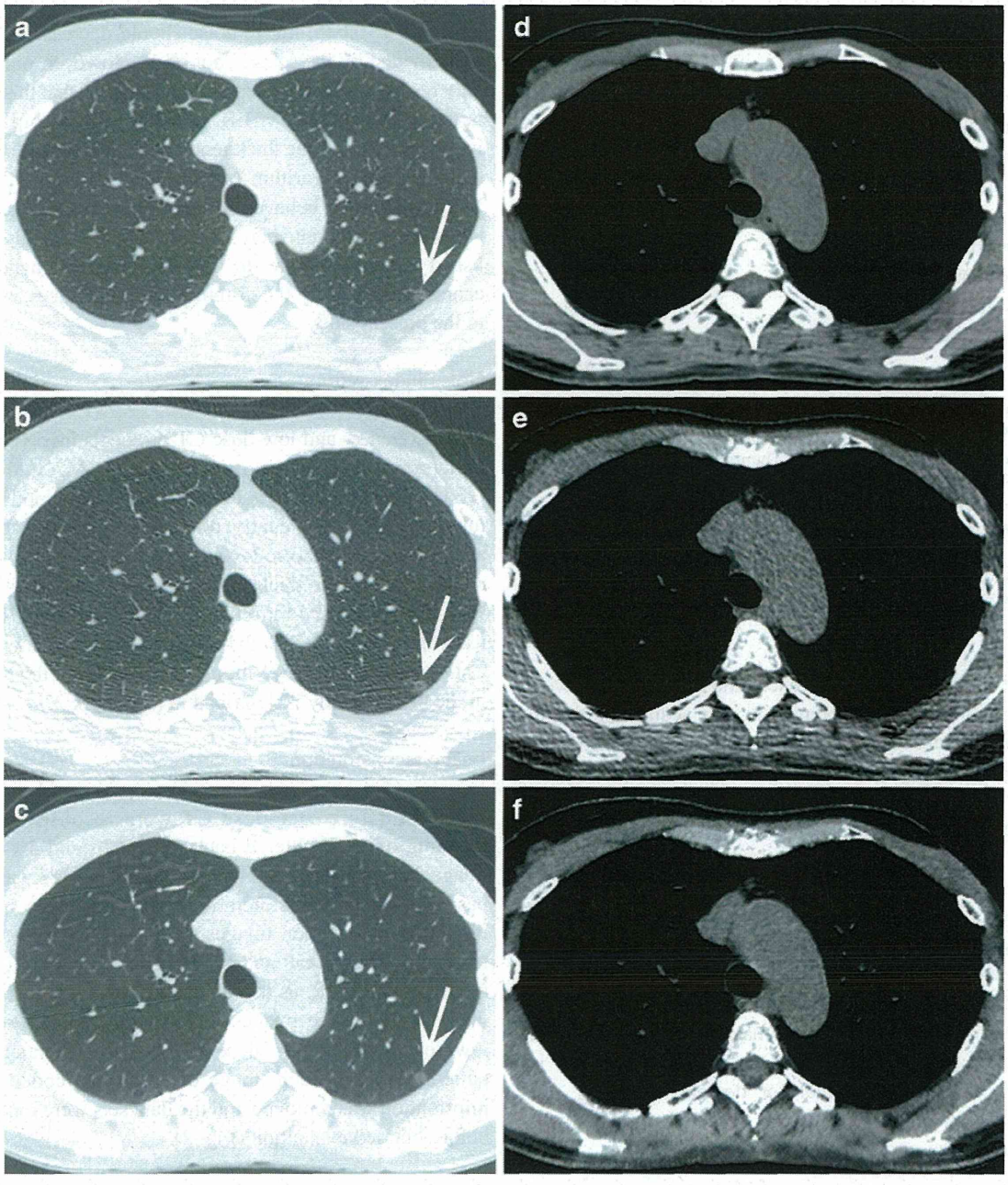

Fig. 1 (a, d) Reference-dose CT images [dose–length product (DLP), 191.10 mGy/cm] reconstructed with adaptive statistical iterative reconstruction (ASIR), (b, e) low-dose CT images (DLP, 38.45 mGy/cm) reconstructed with ASIR and (c, f) low-dose CT images reconstructed with model-based iterative reconstruction (MBIR) in a 58-year-old woman (weight, 50 kg). The prominent streak artefact from the shoulders on low-dose ASIR images (b, e) interferes with adequate visualisation of the ground-glass opacity nodule in the left upper lobe (b, arrow), which renders the image "unacceptable for diagnostic interpretation". Significant improvements in image noise and streak artefacts are observed in low-dose MBIR (c, f), and the nodule is clearly depicted (c, arrow). Low-dose MBIR CT images in this patient have equivalent image quality to reference-dose ASIR CT images (a, d) and were graded as "fully diagnostically acceptable" by both readers. Images are shown in lung [a–c; window width (WW), 1,500 HU; window length (WL), -600 HU] and mediastinal (d–f; WW, 400 HU; WL, 40 HU) window settings

carina (approximately 10 mm in diameter). The mean and standard deviation (i.e. objective image noise) of the CT values (HU) within the ROI were recorded. To evaluate the radiation dose, the estimated CT dose index volume (CTDIvol) and dose–length product (DLP) were recorded for each image data set following completion of the CT examination, according to the dose report. EDs were estimated from DLP using a constant of

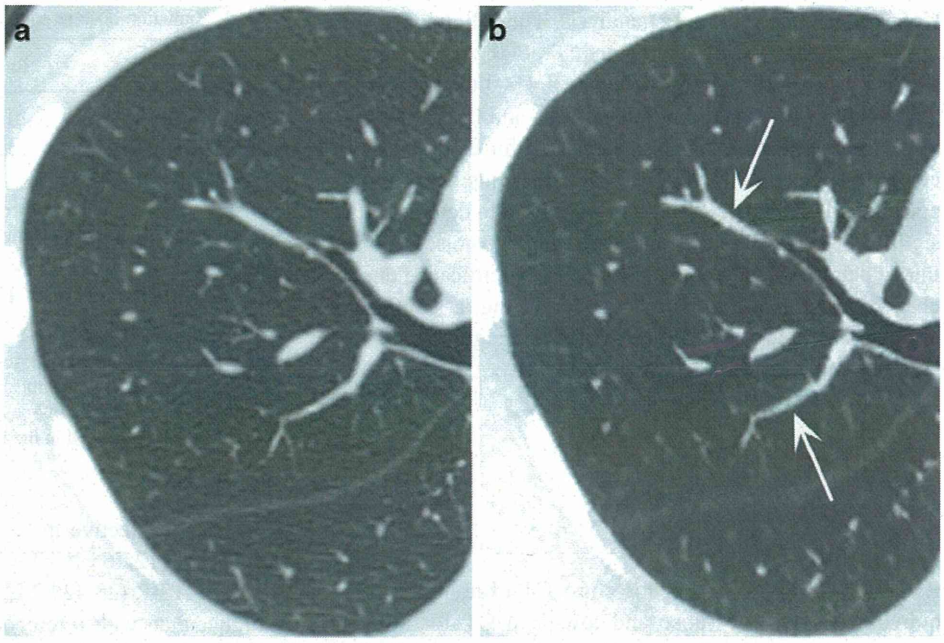

Fig. 2 Reference-dose ASIR (a; CTDIvol, 4.22 mGy; and DLP, 150.43 mGy/cm) and low-dose MBIR (b; CTDIvol, 0.85 mGy; and DLP, 30.24 mGy/cm) chest CT images obtained in a 53-year-old woman weighing 46 kg are shown in the lung (WW, 1,500 HU; WL, -600 HU) window setting. Note the blotchy, pixellated appearance (arrows) in b compared with a

0.014 mSv/mGy-cm as described in the report of the national survey conducted in the UK in 2003 (NRPB W67) [25]. Radiation dose descriptors in the present study were compared with the typical dose described in the NRPB W67 report [25].

Subjective image quality

Two thoracic radiologists (HA and IM) independently assessed the image data sets of 100 patients (300 image sets) for image quality using a commercial software package (EV Insite, PSP Corp., Tokyo, Japan). At the time of the present study, both radiologists already had 2.5 years of experience with ASIR images, which were introduced to our department in January 2009. They had little experience with MBIR images at the time of the present study, although they became familiar with them in the training session. In addition to the default preselected lung window settings [window width (WW), 1,500 Hounsfield units (HU), window level (WL), -600 HU] and mediastinal window settings (WW, 400 HU; WL, 40 HU), radiologists were allowed to change the WW and WL for ease of assessment. Both radiologists were blinded to patient data, clinical information and image reconstruction techniques.

For each image data set, each radiologist graded subjective image noise, artefacts, critical reproduction of visually sharp chest structures and diagnostic acceptability (see Appendix 3 for details). Image quality characteristics assessed in this study have been described in the European Guidelines on Quality Criteria for Computerised Tomography [26] and have been used in multiple previous studies in the radiology literature [13, 14, 16, 17]. To assess intraobserver agreement, 10 patients (30 image sets) were randomly selected from the 100 patients and these 30 images sets were analysed twice. Consequently, 330 image sets were analysed in a blinded and randomised manner by each radiologist.

Estimation of modulation transfer function

To compare the effect of MBIR, ASIR and FBP reconstructions on spatial resolution, we performed a phantom study to estimate the modulation transfer function (MTF) by using the same system used for imaging patients as that described above. A phantom (Catphan 600; The Phantom Laboratory, Salem, NY, USA) with a 28-mm-diameter tungsten wire was imaged at a tube current of 120 kVp, with 200 mA, a helical acquisition mode, a section thickness of 0.625 mm, a 0.5-s gantry rotation time and a standard reconstruction kernel (a proprietary kernel of GE Healthcare). Images were reconstructed with the MBIR technique, with 50 % and 100 % ASIR techniques, and with the FBP technique. The MTF was measured at the iso-centre and 10 cm off centre as the angular average of the two-dimensional Fourier transform of the point spread function in each of the reconstructed image data sets.

Statistical analysis

The data were analysed using JMP 9.0.0 software (SAS Institute, Cary, NC, USA). Whenever possible, results were expressed as the mean±the standard deviation. Inter- and intraobserver agreement for the two radiologists was estimated for the subjective image quality parameters using

Cohen's weighted kappa (κ) analysis. The following κ values were used to indicate agreement: 0.00–0.20, poor agreement; 0.21–0.40, fair agreement; 0.41–0.60, moderate agreement; 0.61–0.80, good agreement; and 0.81–1.00, excellent agreement. A sign test was used for each reader to compare subjective image quality assessments between image pairs. A Student's paired t-test was used to determine the significance of differences in objective image noise between image pairs. To reduce the possibility of significance due to chance because of multiple statistical testing, a Bonferroni correction was applied to the P value and significance was assumed only when the P value was <0.016.

Results

Radiation dose

Radiation dose descriptors for chest CT examinations acquired with reference-dose and low-dose CT for all 100 patients are summarised in Table 2. Compared with reference-dose CT, there was a 79.1 % decrease in CTDIvol and a 79.0 % decrease in DLP with low-dose CT. For direct comparison of the radiation dose with NRPB W67 [25], Table 3 selects out patients weighing 65–75 kg (11 patients; 9 male; age, 71.9±7.9 years; body weight, 67.6±2.2 kg). For these patients, the DLP and ED for reference-dose CT (395.5 mGy/cm, 5.54 mSv) were equivalent to the typical dose described in NRPB W67 for chest CT examinations of adults with a mean weight of about 70 kg (400 mGy/cm, 5.6 mSv) [25]. The ED for low-dose CT (1.13 mSv) was equivalent to the average ED for low-dose CT described in the NLST (1.5 mSv) [24].

Objective image quality

Low-dose MBIR images had significantly lower quantitative image noise in the lung parenchyma (16.93±3.00) than low-dose ASIR images (49.24±9.11, P<0.01) and reference-dose ASIR images (24.93±4.65, P<0.01, Table 4).

Table 2 Comparison of the radiation dose for reference- and low-dose CT

	Reference-dose	Low-dose
CTDIvol (mGy)	7.83±2.14	1.63±1.09
DLP (mGy/cm)	288.8±162.8	60.7±43.5
ED (mSv)	4.04	0.85

Data are mean±standard deviation for each value. CTDIvol=CT dose index volume, DLP=dose–length products, ED=effective dose for chest CT determined using a constant of 0.014 mSv/mGy/cm. Compared with reference-dose CT, there was a 79.1 % decrease in CTDIvol and a 79.0 % decrease in DLP with low-dose CT

Table 3 Radiation dose in patients weighing from 65 to 75 kg

	Reference-dose	Low-dose
CTDIvol (mGy)	10.83±2.92	2.20±0.65
DLP (mGy/cm)	395.5±106.3	80.7±24.5
ED (mSv)	5.54	1.13

Data are mean±standard deviation of each value. CTDIvol=CT dose index volume, DLP=dose–length products, ED=effective dose for chest CT determined using a constant of 0.014 mSv/mGy/cm. For 11 patients weighing from 65 kg to 75 kg (9 male and 2 female, age 71.9±7.9 years, body weight 67.6±2.2 kg), DLP and ED for reference-dose CT were equivalent to the typical dose described in NRPB W67 for chest CT examinations of adults with a mean weight of about 70 kg (400 mGy/cm, 5.6 mSv) [25]. The ED for low-dose CT was equivalent to the average ED for low-dose CT described in the NLST (1.5 mSv) [24]

Conversely, objective image noise in the descending aorta with MBIR (12.76±1.25) was significantly lower than with low-dose ASIR (23.42±3.83, P<0.01), but was significantly higher than with reference-dose ASIR (10.01±1.35, P< 0.01). Mean CT values within the ROI placed in the lung parenchyma or the descending aorta did not differ significantly (P>0.10 for each) among reference-dose ASIR, low-dose ASIR and low-dose MBIR.

Subjective image quality

Interobserver agreement between the two radiologists was excellent (κ=0.81–0.96) for subjective image noise, pixellated blotchy appearance and diagnostic acceptability, whereas it was moderate (κ=0.41–0.52) for motion and streak artefacts. Intraobserver agreement for each reader

Table 4 Objective image quality (mean CT value and image noise) measured within each region of interest

Region of interest	Reference-dose ASIR	Low-dose ASIR	Low-dose MBIR
Lung parenchyma (CT value)	-891.73±27.66	-889.78±28.68	-889.18±28.25
Lung parenchyma (image noise)	24.93±4.65*	49.24±9.11*	16.93±3.00*
Descending aorta (CT value)	38.05±5.21	37.26±7.28	36.86±5.76
Descending aorta (image noise)	10.01±1.35†	23.42±3.83†	12.76±1.25†

Data are mean±standard deviation (in HU). Image noise was expressed as the standard deviation of the CT values within the region of interest. Image noise was significantly lower (*P<0.01, Student's paired t-test) in low-dose MBIR than in reference-dose ASIR images for the lung parenchyma; however, it was significantly higher (†P<0.01) for the descending aorta. Mean CT values location did not differ significantly irrespective of region of interest (P>0.10 for all) among reference-dose ASIR, low-dose ASIR and low-dose MBIR images.